REVISTA MATÉRIA V.29 N.3
ISSN 1517-7076 articles e20240163, 2024

Research on formability of Al-Mg-Sc-Zr alloy based on SLM process

Jiahui Zhang[1], Fan Bai[2], Liuyang Huang[1], Hongge Fu[1], Mengyang Liu[1], Guanghua Zheng[1]

[1]North China Institute of Aerospace Engineering, School of Mechanical and Electrical Engineering. 133 Aimin East Road, Langfang, Hebei, China.

[2]Beijing Institute of Control Engineering, Development Center of On-Board Computer and Electronics. 104 Youyi road, Haidian District, Beijing, China.

e-mail: 1184315411@qq.com, 1071548271@qq.com, 2041740100@qq.com, fhg800922@nciae.edu.cn, 1013331924@qq.com, 1254637484@qq.com

ABSTRACT

The fabrication technology of SLM forming Al-Mg-Sc-Zr alloy is widely used in the lightweight structure design of spacecraft. However, there is a need to optimize the process parameters and heat treatment process. The study analyses the process parameters of SLM on the forming density, microstructure and mechanical properties. The results show that the influence of laser power on the relative density is the greatest, followed by the scanning distance, and the scanning speed is the least. The optimal process parameters of Al-Mg-Sc-Zr are obtained as follows: the laser energy density is 130–140 J/mm^3, laser power is 360 W, scanning speed is 1100 mm/s, and scanning spacing is 80 μm. Finally, samples with an average pore size of 15 μm and a relative induced density of 99.9% were obtained. On this basis, the effects of different annealing systems on the microstructure and mechanical properties were studied. Due to a large amount of second-phase precipitation in the remelting zone, the edge of the molten pool and the bottom, it has a pinning effect, which effectively inhibits recrystallization and grain growth during liquid phase solidification, and no abnormal grain growth occurs during the annealing process. The results show that after low-temperature annealing with 325°C insulation for 4 h, the mechanical properties were significantly enhanced and the maximum ultimate tensile strength (UTS) of the sample could reach 524.89 MPa, the maximum yield strength (YS) of the annealed sample can reach 506.01 MPa, the elongation rate of the annealed sample can reach 5.24%, the dimples and defects at the fracture interface were significantly reduced after annealing.

Keywords: SLM forming; Al-Mg-Sc-Zr alloy; Forming defect; Microstructure; Mechanical properties.

1. INTRODUCTION

Al-Mg-Sc-Zr alloy is widely used in aerospace, transportation, power transmission, machinery manufacturing, nuclear power and construction because of its light specific gravity, high specific strength, low cost, easy processing and corrosion resistance [1, 2]. The formable process of Al-Mg-Sc-Zr alloy using Selected laser melting (SLM) technology was proposed and widely used. However, the microstructure and mechanical properties of the material are greatly affected by the parameters of the formability process and heat treatment. As a result, to obtain both high density and excellent mechanical properties, it is crucial to control microstructure and defects by improving the forming process and optimizing the heat treatment process.

With the continuous in-depth study of aluminum alloy materials, Al-Mg-Sc-Zr has been proposed and widely used as a strengthened aluminum alloy material, which is suitable for the SLM forming process. Selected laser melting (SLM) is one of the metal additive manufacturing technologies (also known as 3D printing), and it is also one of the most widely used and adaptable metal additive manufacturing technologies at present.

The density of Al-Mg-Sc-Zr material samples formed by SLM is affected by laser energy density, laser power, scanning speed and other factors. These factors affect the melting and solidification process of the alloy, change the internal stress in the sample, and then affect the pores, thus changing the density of the formed samples. ZHANG *et al.* [3] noted that by changing the scanning strategy, matrix preheating and remelting treatment can effectively reduce porosity. ABOULKHAIR *et al.* [4] studied the influence of different processing parameters and scanning strategies on porosity and found that the higher the scanning speed, the larger the scanning spacing, resulting in the increase of porosity and the decrease of density, and 99.8% relative density can be

Corresponding Author: Hongge Fu Received on 07/04/2024 Accepted on 22/07/2024

DOI: https://doi.org/10.1590/1517-7076-RMAT-2024-0163

obtained by using the appropriate scanning strategy. DI *et al.* [5] prepared Al-Mg-Sc-Zr alloy with a relative density of 99.2% by SLM, and the laser energy density of 151.52 J/mm^3 is the best technological parameter to achieve the highest relative density. XI *et al.* [6] and others found that the relative density of Al-Mg-Sc-Zr alloy samples can reach 99.4% at the optimum laser power of 300 W, and there are only a few small-sized circular pores caused by an insufficient supply of liquid metal. GU *et al.* [7] obtained Al-Mg-Sc-Zr alloy with relative density of 99.5% under the conditions of laser power of 400 W and scanning speed of 800 mm/s. LI [8] found that Al-Mg-Sc-Zr alloy samples with different laser processing parameters were prepared, and it was found that the changing trend of density, surface morphology, and roughness of the samples was consistent with the increase of laser scanning speed, which all increased first and then decreased with the increase of scanning speed. The forming quality was the best when v = 600 mm/s and the density could reach 99.71%. HAO [9] Al-Mg-Sc-Zr alloy with a density of 99.8% was prepared at scanning speed v = 800 mm/s. CHENG [10] prepared Al-Mg-Sc-Zr alloy with a density up to 99.84% at laser power of 300 W, scanning speed of 800 mm/s and scanning interval of 0.15 mm. The research of alloy density of laser constituency melting technology is deepening and attracting the attention of wide academia and industry. Through the optimization of process parameters, material characteristics, powder performance control, defect control, characterization and evaluation, the density of the alloy is gradually increasing, which provides a better foundation for the application of laser selective melting technology. However, further research is still needed to address complex and diverse problems and to promote the application and development of the technology in a wider range of fields.

Al-Mg-Sc-Zr alloy formed by SLM is an aluminum alloy that can be strengthened by annealing systems. During the heat treatment, Al-Mg-Sc-Zr alloy precipitates mainly Al_3Sc phase and Al_3(Sc, Zr) phase. By adjusting the heat treatment parameters, the phase composition, phase distribution, grain size, and grain boundary characteristics in the alloy can be changed. DI *et al*. [5] found that after heat treatment, the area of fine grains at grain boundaries increased significantly, and the microstructure was characterized by a unique "fan-shaped" heterostructure. SCHMIDTKE *et al.* [11] first used the SLM process to form Al-Mg-Sc-Zr alloy and found that the reinforcing effect of phase precipitation was due to the formation of the shell structure of Zr on the precipitate of rich Sc core, and the tensile strength of the alloy obtained after 325°C aging treatment and 4 h insulation was up to 530 MPa. SPIERINGS *et al.* [12] found a bimodal grain size distribution characteristic in the tissue of SLM forming Al-4.6Mg-0.66Sc-0.42Zr-0.49Mn, presence of Al_3(Sc, Zr) at the pool boundary (Sc, Zr) and Al-Mg-oxide mixed particles as nucleation points for Al-based coagulation. To refine the grains, the higher temperature in the center of the molten pool dissolved most particles, producing the growth of thick columnar crystals. The final obtained static tensile properties over 500 MPa, the mechanical properties are mainly affected by the effect of grain refinement and hardening [13]. MA *et al.* [14], in their study on Al-4.0Mg-0.7Sc-0.4Zr-0.5Mn, found that the precipitation of Al_3Mg_2, Al_6(Fe, Mn) and Al_3(Sc, Zr) led to grain refinement, which improved the yield strength and elongation of the alloy. LI [8], MA *et al.* [14], WANG *et al.* [15] and JIE [16] all found that Al-Mg-Sc-Zr alloy has a biphasic structure with columnar crystals and equiaxed crystals alternately distributed along the forming direction, with fine equiaxed crystals at the boundary of the molten pool and columnar crystals inside the molten pool. GENG *et al.* [17] and TANG *et al.* [18] found that the increase in Mg content would reduce the texture and columnar crystal content of the sample. SHEN *et al.* [19] found that homogenization at 500°C did not increase the solubility of alloy elements, but accelerated the precipitation and recrystallization of Sc/Zr elements; aging at 330°C for 1 h promoted the full precipitation of the second phase of $Al_3(Sc_xZr_{1-x})$. SONG [20] found that with the decrease in scanning speed, the fine equiaxed grain area in the alloy changed, the number of Cu-rich phases precipitated from the bottom of the molten pool increased, the number of initial Al_3(Sc, Zr) grains increased, and the corrosion resistance of the alloy decreased. ZHANG *et al.* [21] found that secondary Al_3(Sc, Zr) precipitation significantly affected the corrosion resistance of Al-Mg-Sc-Zr alloy prepared by SLM, and the heat-treated Al-Mg-Sc-Zr sample prepared by SLM had better corrosion resistance and IGC resistance. LI *et al.* [22] found that the reason why the grain size remains unchanged after aging treatment is that Al_3(Sc, Zr) precipitation will hinder grain growth. In addition, MA *et al.* [23] found that Al_3(Sc, Zr) particles can enhance the stability of microstructure; ZHANG *et al.* [24] found that the high performance of SLM processing Al-Mg-Sc-Zr alloy can be controlled by controlling the distribution of nano-precipitates. SPIERINGS *et al.* [25] found that post-treatment of HIP may lead to grains in some coarse-grained areas, and heat treatment leads to an increase in the density of intragranular $Al_3(Sc_xZr_{1-x})$ particles ≤5 nm.

Heat treatment has a significant effect on the mechanical properties of the alloy. During heat treatment, the properties of Al-Mg-Sc-Zr alloy such as high yield strength, tensile strength, elongation, and hardness can be changed by adjusting the microstructure. After 8 h heat treatment at 325°C, the hardness of Al-Mg-Sc-Zr alloy prepared by DI *et al.* [5] increased by 38.5%, reaching 169 $HV_{0.3}$, YS and UTS increased by 41.3% and 18.1%, reaching 490 ± 9.0 MPa and 533 ± 7.5 MPa respectively, and the elongation decreased slightly, reaching 13.1%. After the Al-Mg-Sc-Zr alloy prepared by XI *et al.* [6] was aged at 325°C for 10 h, YS reached 506.4 MPa, UTS

reached 530.1 MPa, and the elongation was 9.0%. When the SLM samples prepared by GENG *et al.* [17] were aged at 350°C for 1 h, the YS reached the maximum value of 457 ± 10 MPa and the elongation was 27 ± 3%. After aging treatment, the sample prepared by TANG *et al.* [18] has a maximum YS of 476 ± 10 MPa and a maximum microhardness of 175 ± 5 HV. SHEN *et al.* [19] measured that after rapid aging at 330°C for 1 h, UTS was 479 MPa, YS was 441 MPa, elongation at break was 14.5%, and shrinkage was 45%. After aging treatment for 6 h, the compressive yield strength of SLM samples prepared by JIA [26] reaches the maximum, about 555 ± 12 MPa, and YS and UTS are 339 ± 2 MPa and 508 ± 1 MPa, respectively, and their strength is equivalent to that of Al-Mg-Sc-Zr formed by traditional SLM. Jiang Baohang New Materials Co., Ltd. [27] successfully developed super-strength 3D printed aluminum alloy HS5601. The UTS of this alloy in the printed state is usually 460–470 MPa, and the strength is stable above 630 MPa after heat treatment. Compared to traditional casting processes, SLM-formed alloys exhibit significant advantages in design freedom, material utilization, superior performance, flexibility, and production efficiency, making them one of the emerging technologies highly favored in modern manufacturing. For example, according to the research of WEN *et al.* [28], the tensile strength of Al-Mg-Sc-Zr alloy cast by squeeze casting method is only 293 MPa. Although the yield strength of the alloy increased by about 110 MPa after the aging treatment, its strength was not as good as that of the alloy formed by selective laser melting. SLM can achieve lightweight and high-strength design, ensuring the reliability of components under extreme conditions. In contrast, traditional casting methods may not be able to meet these complex performance requirements.

To sum up, the density is an important parameter to characterize the forming quality of the alloy prepared by SLM, which affects the mechanical properties of the material. The density is not only related to the material but also determined by the forming parameters (such as laser power, scanning speed, scanning distance, etc.). Heat treatment will affect the microstructure of the metal, and then change the mechanical properties of the metal. Although scholars at home and abroad have carried out a lot of research on SLM-forming high-strength aluminum alloy materials, the research in this area is not deep enough and needs more research. Therefore, this paper will first study the effects of laser power, scanning speed, scanning spacing and powder coating thickness on the forming density of high-strength aluminum alloy through experiments to find the optimal process parameters. Then, the influence of annealing systems on the microstructure and mechanical properties of Al-Mg-Sc-Zr high-strength aluminum alloy formed by SLM is studied, and the optimal annealing system is found through experiments. This has certain significance for the preparation of high-strength aluminum alloy.

2. MATERIALS AND EXPERIMENTAL PROCEDURES

2.1. Materials

To avoid oxidation, the raw material powder is prepared by inert gas atomized. The chemical composition tests are performed according to the GB/T20975 series standards, and the main chemical composition and actual mass percentage of Al-Mg-Sc-Zr powder are shown in Table 1. The powder particle size distribution curve and powder particle size characterization data are obtained from powder particle size analysis by using the laser particle size analyzer. The apparent density of the powder is 1.40 g/cm^3, the angle of repose is 31° and the material D(10) = 15.13 μm, D(50) = 30.88 μm, D(90) = 54.98 μm. The specific particle distribution is shown in Figure 1, which is photographed by scanning electron microscope (SEM).

2.2. Experimental procedures

The laser selective melting equipment used for forming Al-Mg-Sc-Zr high-strength aluminum alloy material is BLT-S310 developed by Xi ‘an Bolite Additive Technology Co., LTD. The main parameters of the equipment are listed in Table 2.

The density and mechanical properties are largely affected by the process parameters, such as the laser power, scanning speed, scan spacing and layer thickness. To quantitate the relationship between process parameters and density and mechanical properties, A 4-level 6-factor orthogonal experiment was designed, three samples were printed for each parameter. The process parameters are shown in Table 3.

Table 1: Chemical composition of Al-Mg-Sc-Zr alloy powder (wt%).

ELEMENT	Mg	Mn	Sc	Zr	O	Cr	Si	Al
Al-Mg-Sc-Zr	4.36	0.59	0.76	0.45	0.0053	0.0014	0.069	Bal.

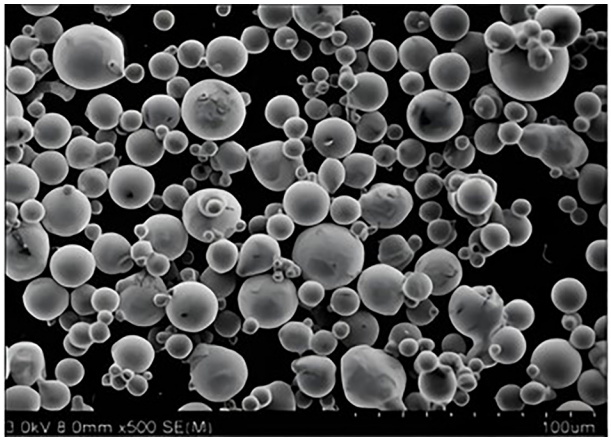

Figure 1: Powder morphologies of the Al-Mg-Sc-Zr alloy.

Table 2: Main technical parameters of the BLT-S310 machine.

PARAMETER	VALUE
The equipment can form the largest size (mm^3)	250 × 250 × 400
Maximum laser power (W)	500
Laser beam wavelength (nm)	1060–1080
Layer thickness (μm)	20–100
Maximum scanning speed (m/s)	7

Table 3: The range of process parameters.

PROCESS PARAMETERS	PARAMETER VALUES
Laser power	270 W, 300 W, 330 W, 360 W, 390 W, 420 W
Scanning speed	950 mm/s, 1000 mm/s, 1050 mm/s, 1100 mm/s, 1150 mm/s, 1200 mm/s
Scan spacing	80 μm, 90 μm, 100 μm, 110 μm, 120 μm, 130 μm
Layer thickness	30 μm

Table 4: Annealing scheme.

NUMBER	ANNEALING SCHEME
1	sedimentary state, without annealing
2	290°C insulation for 4 h and furnace cooling
3	310°C insulation for 4 h and furnace cooling
4	325°C insulation for 4 h and furnace cooling
5	340°C insulation for 4 h and furnace cooling

The annealing scheme directly determines the microstructure and defects of the material. To obtain uniformly refined grain structure and precipitated strengthened phase, the annealing optimization scheme is arranged as shown in Table 4, according to the annealing system of the material.

2.3. Density, morphology, and microstructure detection

The forming samples of Al-Mg-Sc-Zr high-strength aluminum alloy under different process parameters are shown in Figure 2. The forming samples were numbered from 1# to 108#. The density of the SLM forming block is measured by Archimedes drainage method. The equipment used is laboratory precision balance, precision of 0.001 g.

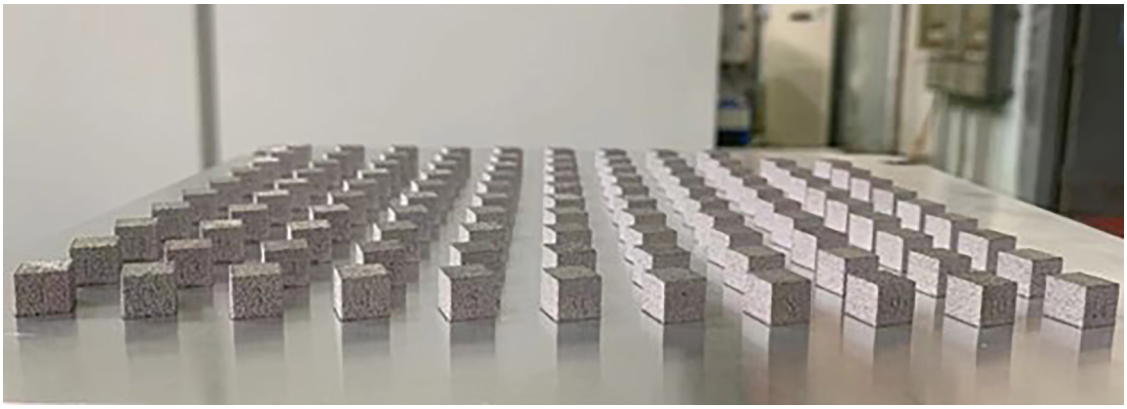

Figure 2: SLM formed samples.

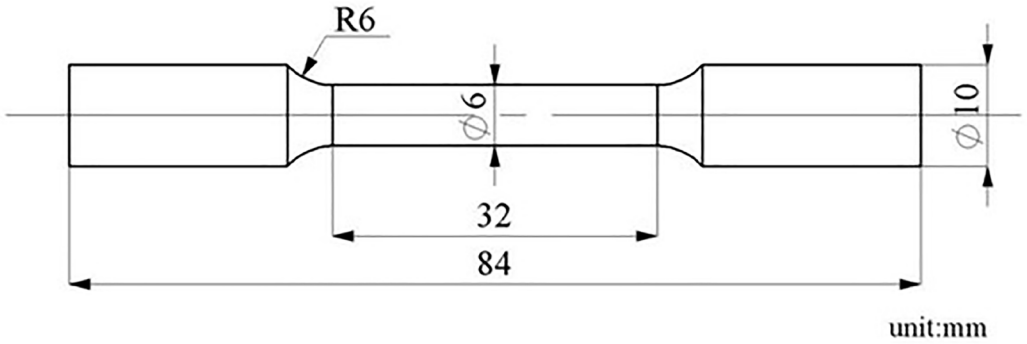

Figure 3: Shape and dimensions of the tensile sample.

The actual density of the sample can be calculated by using Eq. 1 and Eq. 2.

$$\rho_s = \frac{M_2 - M_1}{(M_2 - M_1) - (M_3 - M_4)} \tag{1}$$

$$\rho_x = \frac{\rho_s}{\rho_t} \times 100\,\% \tag{2}$$

Where ρ_s is the actual density of the sample, M_1 is the mass of the copper wire in the air, M_2 is the mass of mass and copper wire, M_3 is the mass of copper wire and mass when immersed in water, M_4 is the mass of the copper wire in the water, and ρ_x is the density of the sample. The theoretical density of Al-Mg-Sc-Zr high-strength aluminum alloy applied in this paper is $\rho_t = 2.69\,\mathrm{g/cm^3}$.

The sample was inserted by the single-cylinder automatic hot-setting machine of METPRESS, and then rough grinding, fine grinding, and fine polishing were carried out by the automatic grinding and polishing machine of EcoMet-300 in turn, and then the sample was corroded by Keller reagent (1.0 ml HF + 1.5 ml HCl + 2.5 ml HNO_3 + 95 ml H_2O) for about 25 s. The morphology and microstructure were analyzed by SEM and optical microscope (OM).

2.4. Mechanical property testing

The mechanical properties were characterized by static tensile test. The experimental equipment is LD26.205 microcomputer control electronic universal testing machine, and the sample size is shown in Figure 3. The test is implemented at room temperature with a tensile rate of 2 mm/min.

As an important index for evaluating mechanical properties, elongation is expressed by δ, which can be expressed in Eq. 3.

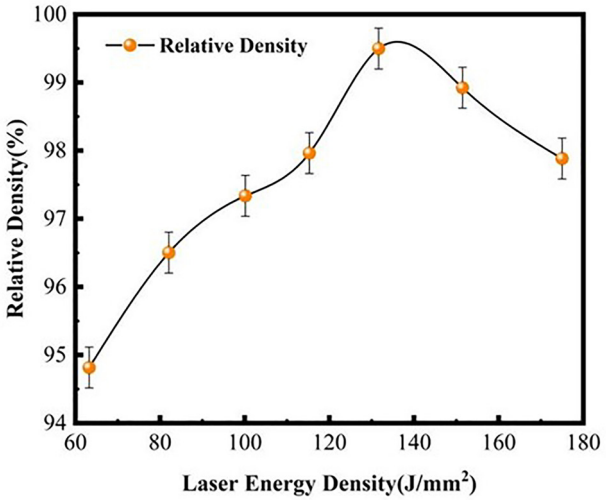

Figure 4: Relation between relative density and laser energy density in SLM molding.

$$\delta = (L_1 - L_0)/L_0 \tag{3}$$

Where L_1 is the mark length after the test rod break, L_0 is the mark length before the test rod breaks.

3. RESULTS AND DISCUSSION

3.1. Densification and porosity defect

Laser energy density is an important influencing factor for the formation of stomata and cracks in metal additive manufacturing [29]. Laser energy density can be divided into line energy density, surface energy density and bulk energy density. To optimize, the process of forming specimen surface integrity, the bulk energy density is used, which can be expressed as Eq. 4.

$$E = P/vdh \tag{4}$$

Where E is the laser energy density, P is the laser power, v is the scanning speed, d is the scan spacing, and h is the layer thickness.

The variation of average density and laser energy input density under the same laser energy input density is measured according to the relative density of the test block. The spline curve obtained by fitting the average density with the laser energy density according to the mean value of the sample points is shown in Figure 4. It can be seen from Figure 4 that the relative density of Al-Mg-Sc-Zr alloy samples prepared by SLM varies significantly at different laser energy densities. It can be seen that when the laser energy density is low, the sample density increases with the increase of laser energy density; however, as the laser energy density continues to increase, the sample density decreases with the increase of laser energy density. When the laser energy density reaches its maximum value of 136.36 J/mm^3, the average density measured by the drainage method reaches 99.9 ± 0.03%. Because selective laser melting is a rapid heating process, when a high-energy laser beam is directly irradiated onto the surface of metal powder, the powder absorbs heat and rapidly heats up and melts, forming a molten pool. When the laser energy density is too low or too high, due to the presence of numerous pores inside the Al-Mg-Sc-Zr alloy samples, the degree of densification is relatively low.

To analyze the influence of each factor on the average density of the test block, an orthogonal test design method was applied. Moreover, the range is obtained for the average density collected by different process parameters (laser power, scanning speed, scanning spacing). As a result, the calculation results are shown in Figure 5. Figure 5(a) shows the highest average density at the laser power of 360 W. Figure 5(b) shows the highest average density at the hatch distance of 0.08 mm. Figure 5(c) shows the highest average density at the scanning speed of 1100 mm/s. The influence factor is R3 > R2 > R1, as can be seen from Figure 5(d). Therefore, in the SLM forming test of Al-Mg-Sc-Zr high-strength aluminum alloy studied in this paper, the influence degree of each forming process parameter on the average density is as follows: laser power > scanning distance > scanning speed.

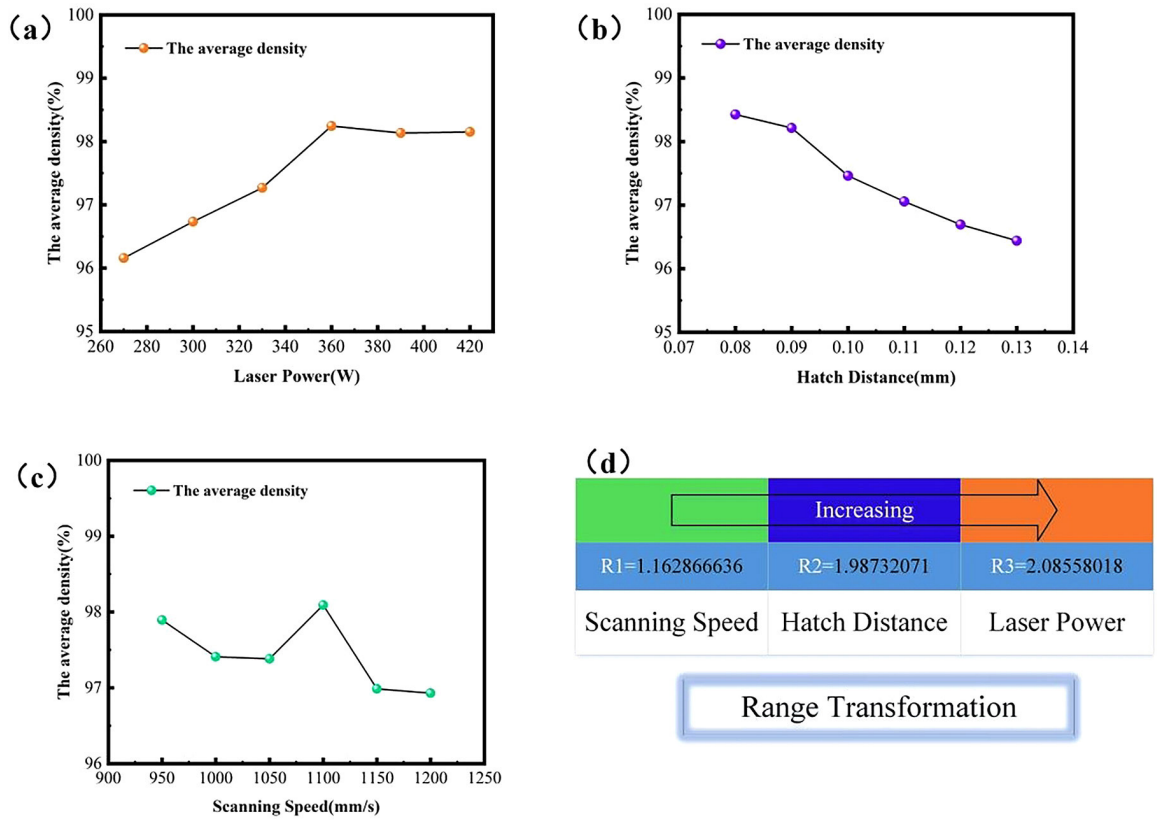

Figure 5: Average density variation curve with different influence factors. (a) The curve of the average density with laser power; (b) the curve of the average density with hatch distance; (c) the curve of the average density with scanning speed; (d) range analysis.

The surface defects and microstructure of Al-Mg-Sc-Zr high-strength aluminum alloy were further observed by a metallographic microscope, and the types and morphology of defects under different process parameters were determined. The mechanism of different defects and the influence of process parameters were summarized. Figure 6 shows the transverse and longitudinal metallographic pictures of SLM-formed Al-Mg-Sc-Zr high-strength aluminum alloy after grinding and polishing under three phases (high 32#, medium 22#, low 6#) input laser energy density.

It can be seen from Figure 6 that the defects on the surface of the sample are mainly holes and no cracks are found, indicating that in the molding process, the scheme is suitable, and the sample has the least defects in the results of the 22# molding process test. At this time, the average size of the defect holes on the X-O-Y plane can be controlled to 13 μm, and the laser energy density E in this case is about 136 J/mm^3. In this case, the corresponding laser power is 360 W, the scanning speed is 1100 mm/s, and the scanning interval is 80 μm. It is found that the morphology of the molten pool on the Y-O-Z surface is closely related to the laser energy density. The Y-O-Z surface of the sample has a typical “Fan-shaped” structure. The formation of pores of Al-Mg-Sc-Zr alloy is mainly due to the injection of high laser energy density, which leads to an increase in the temperature of the melt pool. The water vapor in the powder is decomposed at high temperature, producing more H_2 and metal vapor. During the rapid solidification process of the melt, these gases can escape and remain in the sample in the future. The formation of unfused holes is mainly due to the increased instability of the melt pool at higher laser scanning speeds, which gradually exacerbates the surface spheroidization phenomenon on the melt pool. At the same time, the input of low laser energy also causes the temperature of the melt pool to be relatively low, increasing the surface tension of the molten liquid in the melt pool. In the process of depositing the next layer of metal, the melt cannot fill the pores at the bottom of the large-sized spheroidized particles on the surface of the previous layer of the melt pool, thus forming irregularly shaped or arc-shaped unfused holes at the boundary between the two melt pools. When the laser energy density is too high, the high temperature increases the heat-affected zone of the molten pool. As a result, the powder viscosity decreases. In the flow of the molten pool, the surrounding unmelted particles are combined, resulting in the fusion hole defects of the unmelted particles in the original position. Repeating the above density and defect analysis, it can be seen that when the laser power is about 360 W, the defects on the formed surface are the least.

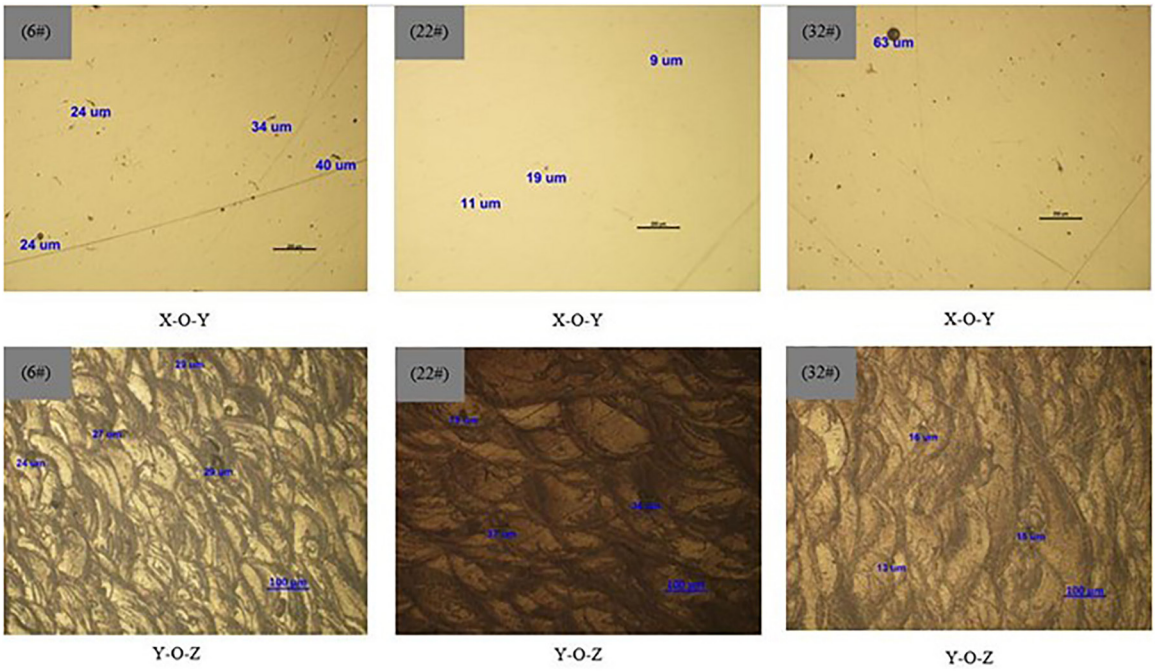

Figure 6: X-O-Y/Y-O-Z forming surface morphology and defect size.

3.2. Microstructures

Heat treatments were performed on the Al-Mg-Sc-Zr specimens according to the experimental design shown in Table 4. SEM microstructures of cross-section after different heat treatments are shown in Figure 7, where (a) is the SEM picture of the sedimentary state, whereas (b), (c), (d) and (e) are the SEM picture of insulation for 4 h at 290°C, 310°C, 325°C and 340°C.

From Figure 7(a) and (b), it can be seen the grains are distributed unevenly. With the increase in temperature, the grains are aggregated and disorderly distribution as seen in Figure 7(c). When the temperature increases up to 325°C or higher than 340°C, the grains are distributed uniformly and there appears clear boundary. As shown in Figure 7(d) and (e). In brief, there is an obvious biphase structure with alternating fine and coarse crystals after annealing. The boundary of the pool is equiaxed crystals, and the interior of the pool is columnar crystals. This phenomenon is not significantly different from the microstructure of the deposited state. This indicates that the grain size was still preserved during annealing and the grain growth was not abnormal. This is because the precipitation of Al_3(Sc, Zr) impedes the growth of grains. However, there is a large number of second-phase precipitation in the remelting zone, the edge and the bottom of the molten pool. The second phase has a pinning effect. It can effectively inhibit the recrystallization and grain growth during liquid phase solidification so that the grains maintain their original size during the heat treatment process. Therefore, the remelting zone, the bottom, and the edge of the molten pool are mainly fine grains. Due to the influence of the temperature gradient, the grains in the molten pool will grow along the temperature gradient towards the top and outside of the molten pool, thus forming columnar crystals. Therefore, the heat treatment refines the grains and makes the microstructure uniform. This eliminates internal stresses and machining defects, thereby reducing hardness and improving machining performance and cold plastic deformation.

3.3. Mechanical properties

3.3.1. Analysis of tensile properties

From what has been discussed in sections 3.1 and 3.2, the average density and the defection perform the best station with the laser power of 360 W and the scanning speed of 1100 mm/s. Moreover, the microstructures in the heat treatment of 4 h at 325°C show uniform and clear boundaries. To further obtain the mechanical properties of the material after different heat treatments, the static tensile test is carried out. Table 5 displays the mechanical properties of Al-Mg-Sc-Zr samples prepared transversely under 360 W-1100 mm/s laser under different heat treatments. The tensile test performed in the text is tensile along the lateral printing. Stress-strain diagram is shown in Figure 8.

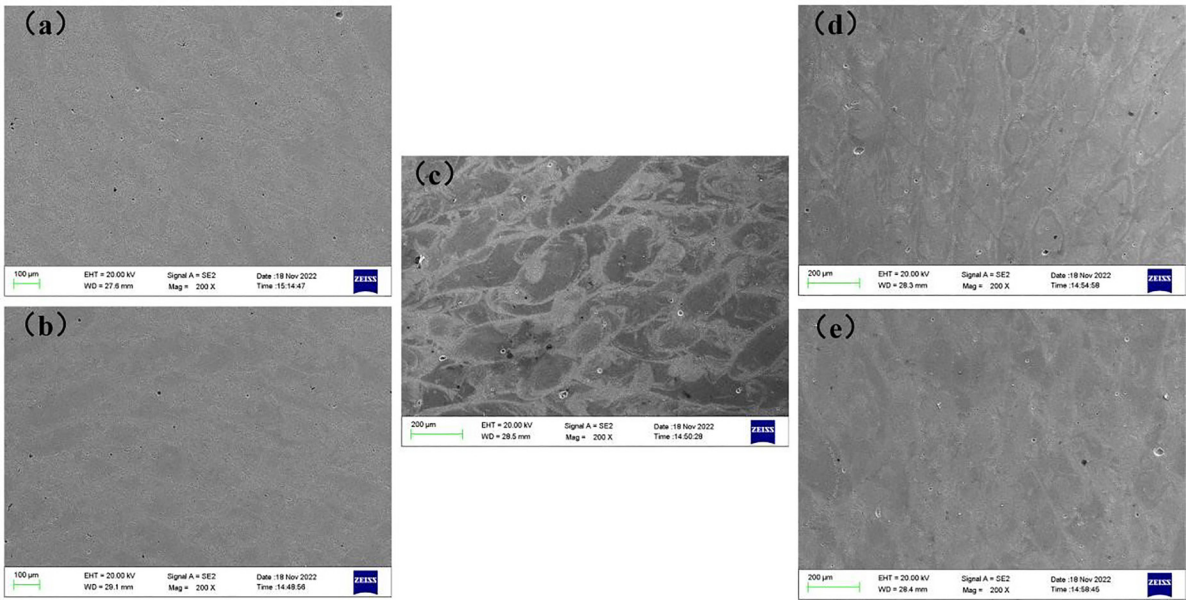

Figure 7: Microstructure of alloy specimens under different annealing systems. (a) Microstructure of Al-Mg-Sc-Zr specimen in sedimentary state; (b) microstructure of Al-Mg-Sc-Zr specimen after annealing at 290°C; (c) Microstructure of Al-Mg-Sc-Zr specimen after annealing at 310°C; (d) microstructure of Al-Mg-Sc-Zr specimen after annealing at 325°C; (e) microstructure of Al-Mg-Sc-Zr specimen after annealing at 340°C.

Table 5: Mechanical properties of transversely formed specimens.

ANNEALING SCHEME	TENSILE STRENGTH (MPa)	YIELD STRENGTH (MPa)	ELONGATION RATE (%)
Sedimentary state	369.22	347.32	11.64
Annealing at 290°C	498.82	465.00	6.18
Annealing at 310°C	509.13	472.15	7.21
Annealing at 325°C	524.89	506.01	5.24
Annealing at 340°C	514.03	483.25	5.10

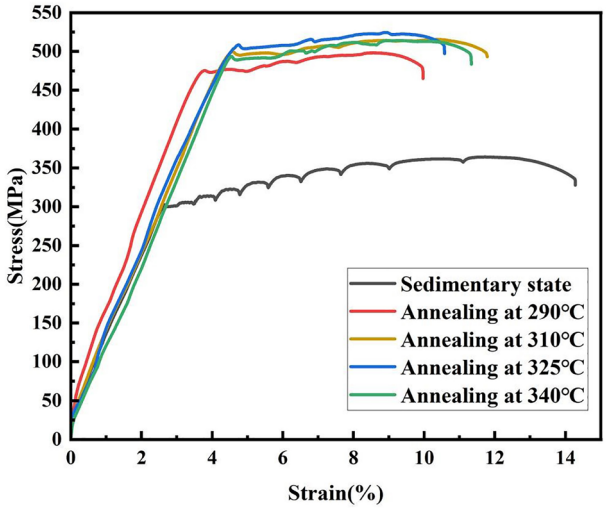

Figure 8: Stress-strain diagram at different annealing temperatures.

It can be seen from Table 5 that in the process of the test rod in the sedimentary state tensile test, UTS and YS of the transverse-formed sample are 369.22 MPa, 347.32 MPa respectively, and the elongation was 11.64%. The optimum annealing system is as follows: After annealing at 325°C for 4 h and cooling in the furnace, UTS, YS and elongation of the transverse formed samples reach 524.89 ± 7.193 MPa, 506.01 ± 6.948 MPa and 5.24%

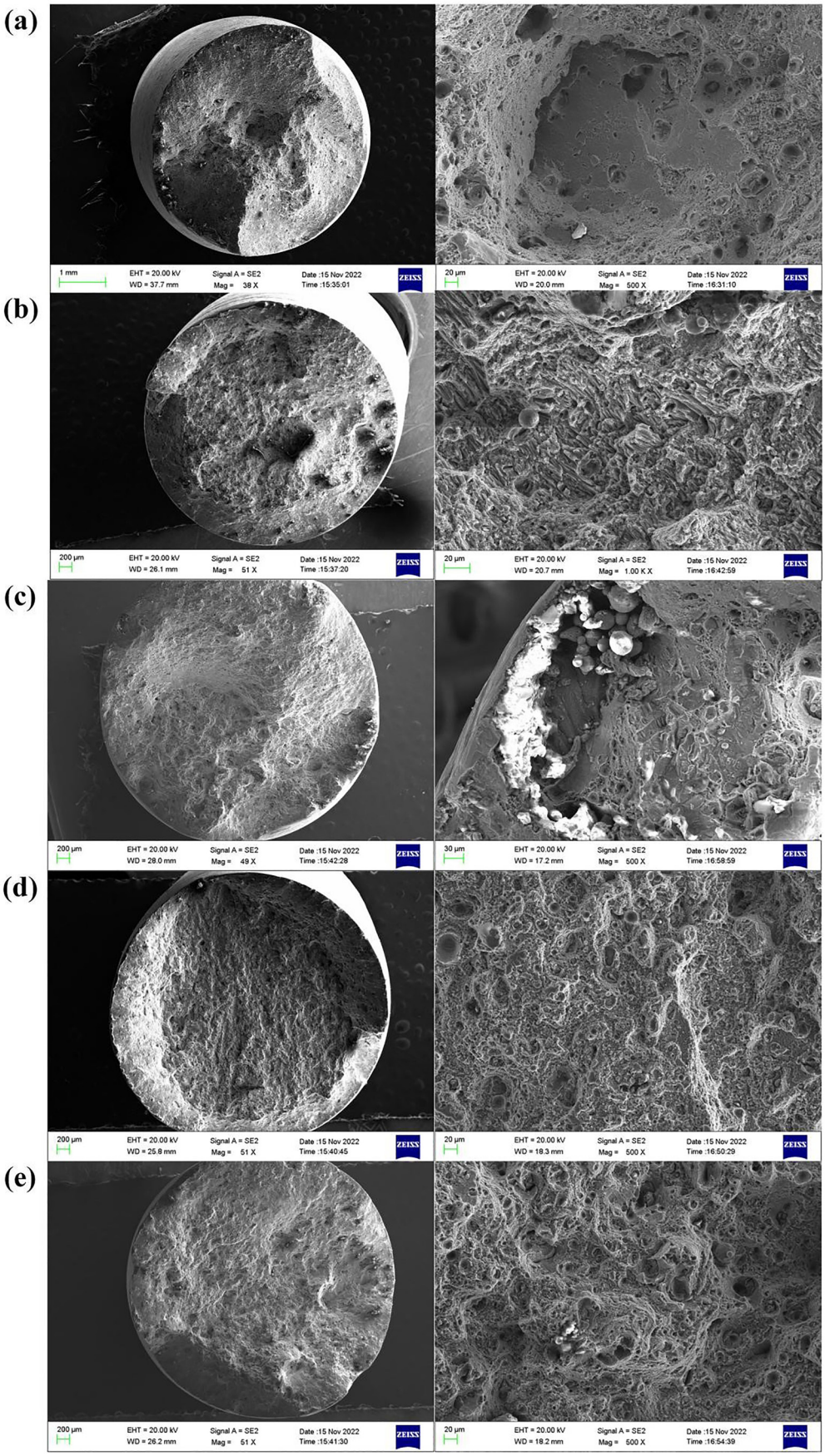

Figure 9: The fracture morphology of SLM-formed samples. (a) The fracture morphology of tensile test rod in sedimentary state; (b) the fracture morphology of tensile test rod after annealing at 290°C; (c) the fracture morphology of tensile test rod after annealing at 310°C; (d) the fracture morphology of tensile test rod after annealing at 325°C; (e) the fracture morphology of tensile test rod after annealing at 340°C.

respectively. Compared with the test rod in the sedimentary state, the tensile strength and yield strength are increased by 42.16% and 45.69%, and the elongation is decreased by 54.98%.

Compared with the deposited Al-Mg-Sc-Zr, the strength of Al-Mg-Sc-Zr formed by SLM after annealing is greatly improved, but the plasticity is somewhat decreased, which is the result of the combined effect of fine crystal strengthening and dispersion strengthening. High laser power promotes the precipitation and refinement of Al_3(Sc, Zr) particles, hindering dislocation movement. Grain refinement is beneficial for improving deformation uniformity and is an effective means to achieve the coordination of alloy strength and plasticity. After annealing, the Sc and Zr elements dissolved in the Al matrix combine to form secondary Al_3(Sc, Zr) particles, which are nailed to the grain boundaries to hinder dislocation movement and improve the strength of the alloy. Compared with the single crystal system of traditional casting and forging aluminum alloys, the average grain size in the mixed crystal structure of SLM-formed Al-Mg-Sc-Zr alloy is significantly reduced. At the same time, the mixed crystal structure of alloy materials is conducive to reducing the unevenness of deformation, and the coarse columnar crystal region can accommodate more dislocations, improving plasticity. The contribution of fine equiaxed grains to mechanical properties lies in promoting deformation uniformity and strength. After SLM forming, comparing the mechanical tensile properties of the test rod after heat treatment, it can be found that the difference of annealing temperature will have a significant impact on the final mechanical properties. However, the strengthening effect at 340°C is better than that at 290°C, which may be due to the high temperature resulting in some Sc and Zr atoms dissolving into the aluminum matrix and failing to form a strengthening phase. It can be seen that while the strength of Al-Mg-Sc-Zr high-strength aluminum alloy is increased after annealing, the plasticity is decreased, but the elongation is still 12.34%. It may be due to the precipitation of a large number of second-phase particles hindering the slipping and twinning of atoms inside the crystal.

3.3.2. Analysis of the fracture morphology

To better analyze the effect of the annealing system on mechanical properties, the fracture of the tensile test rod was also analyzed by SEM. Figure 9 shows the fracture morphology of SLM-formed samples after different heat treatment processes. On the fracture surface, cleavage steps and toughness pits ranging from a few micrometers to tens of micrometers were observed. It can be seen from the microscopic fracture morphology analysis that the annealed fracture presents plastic fracture characteristics, and the main defects of the microscopic fracture include the uneven distribution of holes, unmelted particles and dimpling. This is because Al-Mg-Sc-Zr can absorb more energy and disperse stress through plastic deformation during the tensile process. The dimples are formed before fracture, which indicates that Al-Mg-Sc-Zr has high toughness and ductility. A small amount of unmelted powder particles can also be observed in the fracture surface of the sample, which will form stress concentration at these unmelted defects and hurt the mechanical properties. As shown in Figure 9(d), the fracture dimples of the sample were significantly elongated after being held at 325°C for 4 h, and the direction of the fibers after elongation was consistent, but the number of dimples was significantly reduced compared with the deposited state, so the plasticity decreased. As shown in Figure 9(e), the fracture held at 340°C for 4 h has more dimps than that annealed at 325°C, and the distribution of dimps is relatively uneven and the depth is smaller than that of the deposited state, which is the main reason for the plastic decline.

4. SUMMARY

In this study, Al-Mg-Sc-Zr alloy prepared by laser selective melting (SLM) was studied, the SLM process parameters of Al-Mg-Sc-Zr alloy formed by SLM was optimized, the microstructure of Al-Mg-Sc-Zr alloy under different annealing systems was analyzed, and the corresponding material mechanical performance and the fracture morphology were compared. As a result, the optimum SLM process and annealing system parameters were achieved. The main conclusions are as follows:

(1) In the influence of SLM process parameters, it is concluded that with the increase of scanning speed, the relative density first remains flat, slightly decreases, then increases and then decreases. With the increase of laser power, the relative density of the test block increases and then decreases. The optimal process parameters are shown as follows: laser power P = 360 W, scanning speed v = 1100 mm/s, scanning interval h = 0.08 mm, powder layer thickness μ = 0.03 mm, the laser energy density at this time is about 136.36 J/mm^3. Under these process parameters, the forming sample is in the sedimentary state with a relative density of 99.9%, the UTS ranges from 322 to 375 MPa, and the YS ranges from 301 to 320 MPa.

(2) The microstructure changes of Al-Mg-Sc-Zr high-strength aluminum alloy formed by SLM under five different annealing systems are compared in this paper. The optimal annealing scheme is annealing at 325°C for 4 h. It is found that fine grains are mainly found in the remelting zone, the bottom and edge of the molten pool, and the grains will grow along the temperature gradient towards the top and outside of the molten

pool to form columnar-shaped crystals. With the increase of annealing temperature, the overall properties of Al-Mg-Sc-Zr alloy formed by SLM first increase and then decrease. When the annealing temperature is 325°C, the grain distribution uniformity is improved. The mechanical strength is the highest, UTS can reach 524.89 MPa, and YS can reach 506.01 MPa. UTS and YS were increased by 42.16% and 45.69% respectively. Annealing treatment can effectively improve the strength of the parts and eliminate the residual stress accumulated by the powder thermal effect produced by laser melting.

5. ACKNOWLEDGMENTS

The financial support from Hebei Postgraduate Curriculum Construction Project (KCJSX2024110), Scientific Research Fund project of North China Institute of Aerospace Engineering (YKY202313) and Scientific Research Fund project of North China Institute of Aerospace Engineering (ZD202302).

6. BIBLIOGRAPHY

[1] GUAN, R., LOU, H., HUI, H., *et al*., "Development status, trend and prospect of aluminum alloy materials", *Engineering Science of China*, v. 22, n. 05, pp. 68–75, 2020. doi: http://doi.org/10.15302/J-SSCAE-2020.05.013.

[2] LI, W., FENG, Q., CHENG, X., "Research progress on defects and mechanical properties of high-strength aluminum alloy in additive manufacturing", *Materials & Design*, v. 51, n. 03, pp. 29–38, 2023.

[3] ZHANG, J., SONG, B., WEI, Q., *et al*., "A review of selective laser melting of aluminum alloys: Processing, microstructure, property and developing trends", *Journal of Materials Science and Technology*, v. 35, n. 02, pp. 270–284, 2019. doi: http://doi.org/10.1016/j.jmst.2018.09.004.

[4] ABOULKHAIR, T.N., EVERITT, M.N., ASHCROFT, I., *et al*., "Reducing porosity in AlSi10Mg parts processed by selective laser melting", *Additive Manufacturing*, v. 1–4, pp. 1–4, 2014. doi: http://doi.org/10.1016/j.addma.2014.08.001.

[5] DI, W., FENG, Y., LIU, L., *et al*., "Influence mechanism of process parameters on relative density, microstructure, and mechanical properties of low sc-content Al-Mg-Sc-Zr alloy fabricated by selective laser melting", *Chinese Journal of Mechanical Engineering: Additive Manufacturing Frontiers*, v. 1, n. 4, 2022.

[6] XI, Z., YUAN, T., WANG, M., "Microstructure and mechanical properties of a high-strength Al-Mg-Sc-Zr alloy", *Powder Metallurgy Materials Science and Engineering*, v. 27, n. 02, pp. 205–214, 2022.

[7] GU, D., HAN, Z., GANG, L., *et al*., "Regulation of laser additive manufacturing process of rare earth modified high-strength aluminum micro-truss", *Journal of Aviation*, v. 42, n. 10, pp. 454–466, 2021.

[8] LI, Y., "Study on process optimization and toughness mechanism of laser melting aluminum magnesium scandium and zirconium high strength aluminum alloy", Nanjing University of Aeronautics and Astronautics, 2021. doi: 10.27239/d.cnki.gnhhu.2021.000726.

[9] HAO, T., "Design and properties of Al-Mn-Mg-Sc-Zr alloy", Jiangsu University of Science and Technology, 2021. doi: 10.27171/d.cnki.ghdcc.2021.000028.

[10] CHENG, Z., "Research on laser melting process of Al-Mg-Sc-Zr", China, Academy of Engineering Physics, 2020. doi: 10.27498/d.cnki.gzgwy.2020.000153.

[11] SCHMIDTKE, K., PALM, F., HAWKINS, A., *et al*., "Process and mechanical properties: applicability of a scandium modified al-alloy for laser additive manufacturing", *Physics Procedia*, v. 12, pp. 12, 2011. doi: http://doi.org/10.1016/j.phpro.2011.03.047.

[12] SPIERINGS, A., DAWSON, K., HEELING, T., *et al*., "Microstructural features of Sc- and Zr-modified Al-Mg alloys processed by selective laser melting", *Materials & Design*, v. 115, pp. 115, 2017. doi: http://doi.org/10.1016/j.matdes.2016.11.040.

[13] SPIERINGS, A., DAWSON, K., KERN, K., *et al*., "SLM-processed Sc- and Zr- modified Al-Mg alloy: mechanical properties and microstructural effects of heat treatment", *Materials Science and Engineering A*, v. 701, pp. 701, 2017. doi: http://doi.org/10.1016/j.msea.2017.06.089.

[14] MA, R., PENG, C., CAI, Z., *et al*., "Effect of bimodal microstructure on the tensile properties of selective laser melt Al-Mg-Sc-Zr alloy", *Journal of Alloys and Compounds*, v. 815, n. C, pp. 152422, 2020. doi: http://doi.org/10.1016/j.jallcom.2019.152422.

[15] WANG, Z., LIN, X., KANG, N., *et al*., "Strength-ductility synergy of selective laser melted Al-Mg-Sc-Zr alloy with a heterogeneous grain structure", *Additive Manufacturing*, v. 34, pp. 34, 2020. doi: http://doi.org/10.1016/j.addma.2020.101260.

[16] JIE, L., "Design, preparation and properties study of Al-Mg-(Sc, Z) alloy components specially used for SLM", Jiangsu, Jiangsu University of Science and Technology, 2019. doi: 10.27171/d.cnki.ghdcc.2019.000251.

[17] GENG, Y., HAO, T., LUO, J., "Laser melting formproperties and mechanical properties of Al-Mg-Sc-Zr alloy with high Mg content", *Rare Metal Materials and Engineering*, v. 50, n. 03, pp. 939–947, 2021.

[18] TANG, H., GENG, Y., LUO, J., *et al*., "Mechanical properties of high Mg-Content Al-Mg-Sc-Zr alloy fabricated by selective laser melting", *Metals and Materials International*, v. 27, n. 8, pp. 2592–2599, 2021. doi: http://doi.org/10.1007/s12540-020-00907-2.

[19] SHEN, X.F., CHENG, Z.Y., WANG, C.G., *et al*., "Effect of heat treatments on the microstructure and mechanical properties of Al-Mg-Sc-Zr alloy fabricated by selective laser melting", *Optics & Laser Technology*, v. 143, pp. 107312, 2021. doi: http://doi.org/10.1016/j.optlastec.2021.107312.

[20] SONG, L., "Study on the organization and properties of high-strength Al-3.4Mg-1.08Sc-0.23Zr alloy prepared by laser zone melting", Zhengzhou, Zhengzhou University, 2020. doi: 10.27466/d.cnki.gzzdu.2020.002586.

[21] ZHANG, H., GU, D., DAI, D., *et al*., "Influence of heat treatment on corrosion behavior of rare earth element Sc modified Al-Mg alloy processed by selective laser melting", *Applied Surface Science*, v. 509, n. C, pp. 145330, 2020. doi: http://doi.org/10.1016/j.apsusc.2020.145330.

[22] LI, R., CHEN, H., ZHU, H., *et al*., "Effect of aging treatment on the microstructure and mechanical properties of Al-3.02Mg-0.2Sc-0.1Zr alloy printed by selective laser melting", *Materials & Design*, v. 168, pp. 168, 2019. doi: http://doi.org/10.1016/j.matdes.2019.107668.

[23] MA, R., PENG, C., CAI, Z., *et al*., "Enhanced strength of the selective laser-melted Al-Mg-Sc-Zr alloy by cold rolling", *Materials Science and Engineering A*, v. 775, n. C, pp. 138975, 2020. doi: http://doi.org/10.1016/j.msea.2020.138975.

[24] ZHANG, H., GU, D., YANG, J., *et al*., "Selective laser melting of rare earth element Sc modified aluminum alloy: thermodynamics of precipitation behavior and its influence on mechanical properties", *Additive Manufacturing*, v. 23, pp. 23, 2018. doi: http://doi.org/10.1016/j.addma.2018.07.002.

[25] SPIERINGS, A., DAWSON, K., DUMITRASCHKEWITZ, P., *et al*., "Microstructure characterization of SLM-processed Al-Mg-Sc-Zr alloy in the heat treated and HIPed condition", *Additive Manufacturing*, v. 20, pp. 20, 2018. doi: http://doi.org/10.1016/j.addma.2017.12.011.

[26] JIA, C., "Study on formproperties and properties of SLM Al-Mg-Mn-Er-Zr alloy", *Jiangsu, Jiangsu University of Science and Technology*, 2022. doi: 10.27171/d.cnki.ghdcc.2022.000036.

[27] LI, YONGCHUN, YIN, JIANPING, *et al.*, "Domestic 600 MPa ultra high strength 3D printed aluminum alloy", *Aluminum Processing*, v. 2, pp. 22, 2022.

[28] WEN, Y., DU, G., YAN, D., *et al*., "The effect of squeeze casting on the microstructure and mechanical properties of Al-Mg-Sc-Zr alloy", *Special Casting and Nonferrous Alloys*, v. 34, n. 1, pp. 1–6, 2014.

[29] LI, R., LIU, J., SHI, Y., *et al*., "Balling behavior of stainless steel and nickel powder during selective laser melting process", *International Journal of Advanced Manufacturing Technology*, v. 59, n. 9–12, pp. 1025–1035, 2012. doi: http://doi.org/10.1007/s00170-011-3566-1.